Polymer 49 (2008) 2328–2333

Contents lists available at ScienceDirect

Polymer

journal homepage: www.elsevier.com/locate/polymer

Interfacial polarization phenomenon in the recrystallization of poly(butylene succinate)

Horng-Jer Tai *

Department of Chemical Engineering, I-Shou University, Number 1, Hsueh-Cheng Road, Section 1, Ta-Hsu Hsiang, KaoHsiung County 84008, Taiwan

ARTICLE INFO

Article history:
Received 12 December 2007
Received in revised form 12 March 2008
Accepted 15 March 2008
Available online 19 March 2008

Keywords:
Interfacial polarization
Poly(butylene succinate)
Recrystallization

ABSTRACT

The Maxwell–Wagner–Sillars relaxation behavior of poly(butylene succinate) during melting and recrystallization at 383 K was studied. It was found that the polarization originates from the three-phase structure of the dispersion of spherulites in the crystallizing melt. A model made up of a conductive melt matrix and a dispersion of spherical semicrystalline particles was proposed. The semicrystalline particles were composed of continuous, nonconductive crystals and spherical amorphous inclusions with the conductivity of the melt matrix. The three-phase Bruggeman–Hanai theoretical equations for interfacial polarization were employed and the relaxation behavior were successfully simulated. Three parameters – the melt conductivity, the volume fraction of the semicrystalline particles, and the amorphous fraction within these particles are obtained by fitting the theoretical equations to the experimental data. Their relationships with the morphological development during the recrystallization process were correspondingly discussed.

1. Introduction

Poly(butylene succinate), PBSu, is a biodegradable synthetic aliphatic polyester that has an interesting simultaneous melting and recrystallization behavior, which leads to the occurrence of multiple melting peaks in calorimetric spectra [1–4]. Although PBSu has two polymorphs [5–7], the α and β crystal forms, the aforementioned melting peaks are associated with the melting of the α crystal. The β crystal can be found only when the material is under strain [5]. In their study, Yoo et al. showed the existence of two morphologically different crystallites that underwent a melting-recrystallization process when PBSu was crystallized isothermally [4]. Qiu et al. reported on the prominent melting-recrystallization behaviors when PBSu was crystallized non-isothermally [2] or isothermally [3]. Moreover, Yasuniwa et al. studied the melting-recrystallization behaviors of PBSu resins of three different molecular weight distributions. Their study revealed that the height of the high-temperature melting peak decreased with the increasing molecular weight, while that with low-temperature melting peak increased [1]. It was attributed to the lower recrystallization rate for PBSu with higher molecular weight.

In another work on dielectric investigation of PBSu [8], the researcher of the present study could clearly observe the melting-recrystallization behavior, which caused a dielectric relaxation due to interfacial polarization. Interfacial or Maxwell–Wagner–Sillars (MWS) polarization can occur in a multiphase system because its components have different dielectric constants and electrical conductivities. The magnitude of this polarization and its dispersion behavior depend not only on material properties but also on volume fraction, geometrical shape, and the orientation of each constituent phase. Remarkable dielectric dispersion due to MWS interfacial polarization can be found in biological cells and tissues [9], composites [10–12], organic dye–polymer mixtures [13] and many other heterogeneous systems [14]. Interfacial polarization is caused by the piling up of space charges in the volume or at the interface because of the difference in conductivities among the constituent phases when an oscillatory electric field is applied [15]. Dielectric relaxation spectroscopy (DRS) has long been used to study polymer crystallization processes, but reports focused on interfacial polarization phenomena upon crystallization are scarce. In the thermoplastic polyester family, poly(ethylene terephthalate) (PET) has especially received much attention. PET has the advantage in that it can be prepared in a completely amorphous state as well as in a semicrystalline state. Fukao and Miyamoto [16,17] studied the change in the α relaxation function of the PET crystallized near its glass transition temperature. Initially, the relaxation function followed the Kohlrausch–Williams–Watts equation, and then changed into the Cole–Cole equation upon isothermal cold crystallization. Before an ordered crystalline structure was formed during the isothermal process, a transition of the polymer – from its glassy to disordered state with higher thermal fluctuation – had been found. The α relaxation associated with the glassy state changed into the α′ process

* Tel.: +886 7 6578901; fax: +886 7 6578945.
E-mail address: hjtai@isu.edu.tw

0032-3861/$ – see front matter © 2008 Elsevier Ltd. All rights reserved.
doi:10.1016/j.polymer.2008.03.025

associated with the semicrystalline state during the transition period. Thereafter, crystallization began to produce a normal crystalline and higher-order structure. In their study, Sics et al. used a simultaneous small angle X-ray scattering (SAXS) and dielectric spectroscopy technique to observe the cold crystallization process of PET from an amorphous state [18]. The researchers reported simultaneous changes in the maximum dielectric loss value of α relaxation, the degree of crystallinity, the Lorentz corrected integrated SAXS intensity, and the long spacing of the lamellar stacks. Boyd et al. observed an MWS interfacial polarization effect from their dielectric permittivity curve for semicrystalline PET, which was absent for its amorphous counterpart [19]. The researchers did not go any further into the detail. The space charge-related effects in biaxially stretched PET films were studied by Neagu et al. [20]. The researchers found that the DC conductivity followed the Vogel–Fulcher–Tammann (VFT) equation and concluded that the charge carrier transport mechanism was governed by the motion of the polymer chains.

In his previous study on interfacial polarization, the researcher of the present study explained the phenomenon during recrystallization of PBSu based on a phenomenological approach [8]. The dielectric spectra were analyzed using an equivalent circuit model, in which the MWS relaxation was represented by a Cole–Cole element. The parameters, such as relaxation time and relaxation strength, changed upon recrystallization, but how these changes were related to morphological evolution was not well understood. In this article, these data had been reanalyzed based on the developed dielectric theories for interfacial polarization. In doing so, the researcher hoped that the results would help in understanding the relationship between MWS relaxation behaviors and morphological developments upon recrystallization. In addition, the researcher believed that the methodology he followed in this study could be adopted in future research on the same subject.

2. Experimental

The PBSu resin used was Bionolle #1001 that was supplied by Showa Highpolymer Co., Ltd. The PBSu pellets were dried at 343 K for 4 h and then were melt-processed at 453 K for 3 min using a Brabender Plasti-Corder PL2000 equipped with roller blade rotors. The melts were transferred to a compression molding machine preset at the same temperature. When the melts were heat pressed into films for 3 min, the heating platens were water-cooled to 363 K. The films were allowed to crystallize at 363 K for 2 h. Those films which were about 100-μm were then prepared. DRS measurements in the frequency range of 0.01–10^5 Hz were carried out by means of a TA Instruments DEA 2970 dielectric analyzer. During the continuous isothermal frequency sweep measurements, the 363 K crystallized samples were heated up to 383 K and 393 K successively, and were held at each temperature for about 7 h. Subsequently, the samples were heated up to 403 K, with one isothermal frequency scan taken. More experimental details can be found in Ref. [8].

3. Results and discussion

The dielectric properties of materials may be expressed in different formalisms [21]: dielectric permittivity relative to vacuum ε^*, electrical modulus M^*, electrical conductivity σ^*, and electrical resistivity ρ^*. The inter-relationships between these quantities are expressed as follows:

$$\varepsilon^* = \frac{1}{M^*} = \frac{\sigma^*}{j\omega\varepsilon_v} = \frac{1}{j\omega\varepsilon_v\rho^*} \tag{1}$$

where ε_v is the permittivity of vacuum, ω is the angular frequency, and $j = (-1)^{1/2}$. The complex permittivity of the recrystallizing PBSu was expressed in Ref. [8] via:

$$\varepsilon^* = \varepsilon_\infty + \frac{\Delta\varepsilon}{1+(j\omega\tau)^\alpha} + \frac{\sigma_o}{j\omega\varepsilon_v} \tag{2}$$

where ε_∞ is the limiting high frequency permittivity, $\Delta\varepsilon$ is the amplitude of the MWS polarization, α is the stretching exponent for the Cole–Cole element, τ is the median MWS relaxation time, and σ_o is the bulk ionic conductivity. All parameters in Eq. (2) changed during recrystallization, with each parameter changing in a different pattern and extent. $\Delta\varepsilon$ grew from 0 to 50; σ_o also experienced a five-fold decrease from 8.1 to 1.6 μS/m and so on. The dispersion data will be re-examined using a different approach. Fig. 1 shows the dispersions of the real parts of ε^* and σ^* of PBSu melt at three varying temperatures. The reported melting point of PBSu was 387 K. The curves for 383 K are the initial dispersion curves when PBSu experienced massive melting while recrystallization had not begun yet. The curves for 393 K are the representative curves, and very little change in the curves was observed throughout the 4 h frequency scanning period. The dispersion behaviors at the three temperatures were similar. At high frequencies, little dispersion was observed for both ε' and σ', and the material behaved like a dielectrically lossless material with a frequency-independent, real dielectric permittivity ε that showed conduction because of space charges. The two quantities, ε^* and σ^* are just

$$\varepsilon^* = \varepsilon + \frac{\sigma}{j\omega\varepsilon_v} \tag{3}$$

$$\sigma^* = \sigma + j\omega\varepsilon_v\varepsilon \tag{4}$$

where σ is the DC conductivity. In terms of equivalent circuit, the material within this (high) frequency range can be represented as a parallel pair of resistor and capacitor. At frequencies lower than 10^3 Hz, the electrode polarization effect sets in and ε' increased dramatically. At high frequencies, σ' assumed the value of DC conductivity because the charge species migrated in rhythm with the AC field and made small excursions. At frequencies lower than 10 Hz, the excursions became so large that the migration of the charge species was hindered by the double layers formed at the metal electrode–polymer interfaces and σ' began to decrease [22]. It can also be seen clearly that σ' was less sensitive to electrode polarization than ε'.

Fig. 2 shows the variations in ε' and σ' with time as recrystallization took place at 383 K. Because the temperature was

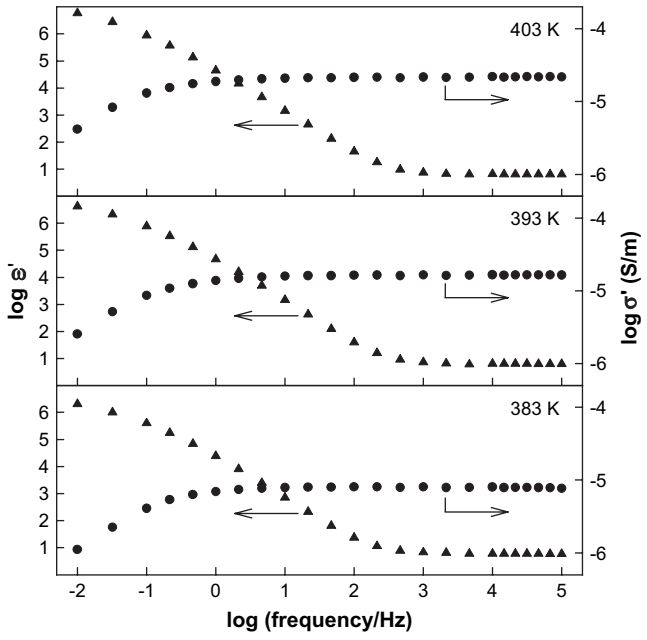

Fig. 1. Real permittivity ε' and conductivity σ' of PBSu at the three temperatures.

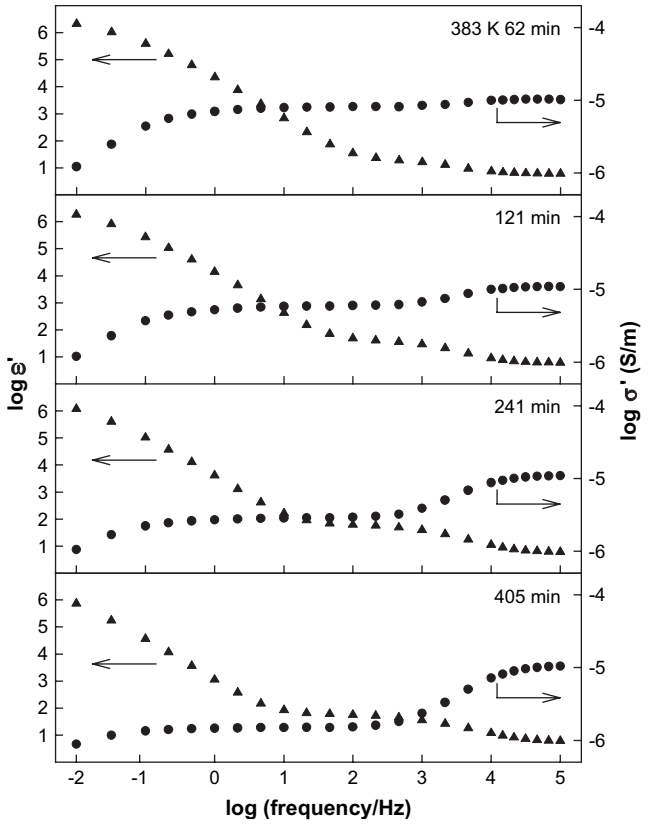

Fig. 2. Real permittivity ε' and conductivity σ' of PBSu at recrystallization times of 62, 121, 241 and 405 min at 383 K.

very close to the melting temperature, the rate of recrystallization was very low. Compared with the 383 K curves in Fig. 1, the changes that occurred in the frequency range between 10 and 10^4 Hz were quite dramatic (step changes were introduced to both the ε' and the σ' curves), that is, a simple dispersion process occurred upon recrystallization, causing the conductivity (σ') to reduce and the high frequency permittivity to increase. The dispersion was attributed to an MWS interfacial polarization caused by the formation of crystalline phase [8].

The theoretical expressions for the dielectric properties of a heterogeneous mixture have long been developed and compiled [23,24]. Successful applications of these theories to heterogeneous polymer systems have been reported in many occasions. For instance, Hayward et al. reported the remarkable agreement between theoretical predictions and experimental observations for a series of model systems composed of conductive poly(ethylene oxide) inclusions in a polycarbonate matrix [14]. Furthermore, Boersma et al. succeeded in calculating the shape of liquid crystalline polymer inclusions inside a polypropylene matrix; they did so by applying theoretical analysis on the dielectric spectra together with microscope observations [25]. Based on a composite material approach, the dielectric permittivity ε^* of a dilute suspension of randomly oriented ellipsoids in a matrix can be expressed as follows [24]:

$$\varepsilon^* = \varepsilon_a^* \left[1 + \frac{1}{3}\phi \sum_{k=x,y,z} \frac{\varepsilon_p^* - \varepsilon_a^*}{\varepsilon_a^* + \left(\varepsilon_p^* - \varepsilon_a^*\right) L_k} \right] \tag{5}$$

where L_k is the depolarization factor along the k-axis, ε_a^* and ε_p^* are the dielectric permittivities of the matrix and the ellipsoids, respectively, and ϕ is the volume fraction of the ellipsoids. For the concentrated dispersion of spherical particles, where $L_k = 1/3$, Hanai extended Bruggenman's equation for electrical conductivity and derived the following equation through the integration of Eq. (5) for an infinitesimally small amount of the dispersed phase to higher volume fractions (the Bruggeman–Hanai equation) [24,26]:

$$1 - \phi = \left(\frac{\varepsilon^* - \varepsilon_p^*}{\varepsilon_a^* - \varepsilon_p^*} \right) \left(\frac{\varepsilon_a^*}{\varepsilon^*} \right)^{1/3} \tag{6}$$

In Hanai's experiments and theoretical analysis, the dispersion in ε' and σ' for oil-in-water type emulsions were very small, while the dispersions were much larger for water-in-oil type emulsions, especially for those with high water content. The dielectric dispersion spectra for a crystallizing polymer should resemble those obtained for the oil-in-water type emulsions because the emerging crystal phase is much less conductive, and the initial polymer melt acts as a continuous, more conductive matrix. However, this will be inconsistent with Hanai's theoretical prediction because large dispersions due to interfacial polarization were observed experimentally for PBSu. On the other hand, calculations based on the water-in-oil material model using Eq. (6), which would predict a much larger dispersion in both ε' and σ', also failed to give a reasonable account of the experimental data.

Looking at the crystallization process more closely, one can clearly see that this crystalline particles–amorphous melt matrix, two-phase model is too oversimplified. The crystallization of a polymer often proceeds through spherulitic conversion [7]. A spherulite is a two-phase entity. This means that a three-phase material model will simulate a crystallizing polymer better. One of the simplest three-phase material models was adopted in this study; the recrystallization of PBSu was considered as a suspension of spherical semicrystalline particles containing spherical amorphous inclusions, dispersed in the continuous melt matrix. Eq. (6) can again be used to calculate the dielectric permittivity ε_p^* of the semicrystalline particles [24]:

$$1 - \nu = \left(\frac{\varepsilon_p^* - \varepsilon_1^*}{\varepsilon_2^* - \varepsilon_1^*} \right) \left(\frac{\varepsilon_2^*}{\varepsilon_p^*} \right)^{1/3} \tag{7}$$

where ε_1^* and ε_2^* are the dielectric permittivities of the amorphous inclusions and the continuous, crystalline phase within the particle, respectively, and ν is the volume fraction of the amorphous inclusions within the semicrystalline particle. The degree of crystallinity can then be calculated by

$$X_\varepsilon = \phi \times (1 - \nu) \tag{8}$$

where X_ε denotes the crystallinity obtained from the dielectric technique. Eq. (7) is a cubic function: ε_p^* can be analytically solved and expressed in terms of ε_1^*, ε_2^*, and ν. Similarly, ε^* in Eq. (6) can be expressed in terms of ε_a^*, ε_p^*, and ϕ. Using the nonlinear fitting technique, one can obtain the parameters such as the conductivity and the dielectric permittivity of each constituent phase, ϕ, and ν. For simplicity, it can be assumed that the amorphous inclusion inside the semicrystalline particle had the same dielectric permittivity and conductivity as the bulk external melt phase. Because the focus in this research was on the MWS interfacial polarization and the dipolar loss was negligible compared with the conduction loss, the complex permittivities of the melt and the amorphous inclusion can then be expressed as

$$\varepsilon_a^*(\omega) = \varepsilon_1^*(\omega) = \varepsilon_m + \frac{\sigma_m}{j\varepsilon_v \omega} \tag{9}$$

where ε_m and σ_m are the high frequency (relaxed) permittivity and DC conductivity of the melt, respectively. Interfacial polarization arose primarily from the difference in mobility of charge species in the crystalline and noncrystalline phases of PBSu, and the ionic conductivity of the crystalline phase should be much less than that of the melt. The difference between the dielectric permittivities of the melt and the crystalline phases was too small to make

a significant contribution to the polarization. Therefore, it was further assumed that the DC conductivity of the crystalline phase was 0 and the dielectric permittivity was equal to that of the melt. That is,

$$\varepsilon_2^*(\omega) = \varepsilon_m \tag{10}$$

The high frequency, relaxed dielectric permittivity for PBSu melt at 383 K at the beginning of recrystallization was 6.15 [8] and was used as ε_m in Eqs. (9) and (10). It was actually the ε_∞ in Eq. (2), which was assumed to remain constant throughout the entire recrystallization process. This made the number of fitting parameters to only three: σ_m, ϕ, and ν. One can note, too, that the above assumptions can be relaxed as long as there are enough experimental data points to justify the numerical fitting.

Fig. 3 shows the comparisons of the theoretical calculations and the experimental data for the recrystallization spectra at 383 K at various times. In Fig. 3, the results are presented in Cole–Cole plots using the electrical resistivity formalism, which is the best way to show the transition in dielectric spectra during recrystallization and to see the effectiveness of the fitting. The same figure also shows the frequency ranges, which were carefully chosen so that the electrode polarization effect could be neglected. As can be seen, despite the simplicity of this material model, the agreement between the theoretical predictions and the experimental data was very good. Initially (recrystallization time = 0 min), a simple semicircle can be seen, a characteristic of an ion-conducting dielectric represented as a parallel pair of resistor and capacitor as explained in the three plots in Fig. 1. As recrystallization proceeded, another arc stemmed from the semicircle. This new process was, of course, the MWS interfacial polarization which led to a great change in conductivity (and resistivity) as crystallinity increased. In terms of equivalent circuits, it introduces an additional Cole–Cole element as expressed in Eq. (2). As can be seen, this arc grows in size, becomes skewed, and overshadows the initial semicircle at later stages. The interfacial polarization effect can also be observed by using the electrical modulus formalism. In the Cole–Cole plot for M^*, however, the semicircle due to interfacial polarization is always overshadowed by the much larger initial semicircle and is less discernible, especially at low crystallinity. A series of material models with different geometrical arrangements between crystalline and amorphous phases inside the semicrystalline particle were also tried. For a shell–sphere, the dielectric permittivity ε_p^* is expressed as follows [24]:

$$\varepsilon_p^* = \varepsilon_2^* \frac{2(1-\nu)\varepsilon_2^* + (1+2\nu)\varepsilon_1^*}{(2+\nu)\varepsilon_2^* + (1-\nu)\varepsilon_1^*} \tag{11}$$

and for two layers in series structure

$$\frac{1}{\varepsilon_p^*} = \frac{1-\nu}{\varepsilon_2^*} + \frac{\nu}{\varepsilon_1^*} \tag{12}$$

The predicted values using the fitted parameters based either on Eqs. (6) and (11) or Eqs. (6) and (12) compared much less favorably to the experimental data than when Eqs. (6) and (7) were used, as shown in Fig. 4. The Cole–Cole plots of the 405 min dispersion using both the electrical resistivity and the modulus formalisms were compared for the three geometrical models: spherical particles with spherical amorphous inclusions (Eqs. (6) and (7)), with a crystalline shell (Eqs. (6) and (11)), and with a planar layer structure (Eqs. (6) and (12)). Table 1 shows the obtained fitting parameters for the three models. The deviations are visually accentuated in the modulus formalism. The sum of squares of the residuals for the spherical inclusions, the crystalline shell, and the layered structure are 1.7×10^{-4}, 1.9×10^{-3}, and 1.2×10^{-3}, respectively. The geometrical model with spherical amorphous inclusions apparently outperformed the other two models. Therefore, the geometrical model was chosen for the analysis of the MWS polarization. The two layers in parallel model, where $\varepsilon_p^* = \nu\varepsilon_1^* + (1-\nu)\varepsilon_2^*$, were also tested. Two additional parameters, the permittivities of the amorphous and the crystalline phases, were needed to achieve a good fit. The obtained permittivity values were unreasonable, with the amorphous permittivity less than 1, and the crystalline permittivity larger than 20. This model was thus discarded. Because the stacks of

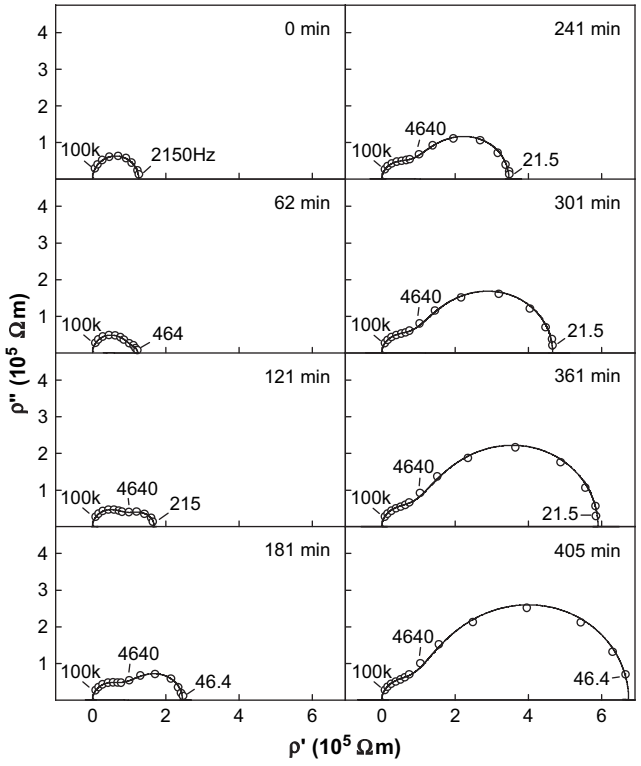

Fig. 3. Cole–Cole plots of electrical resistivity ρ^* at several recrystallization times at 383 K. The solid lines are the calculated values using Eqs. (6) and (7). Numbers along the curves are the frequencies.

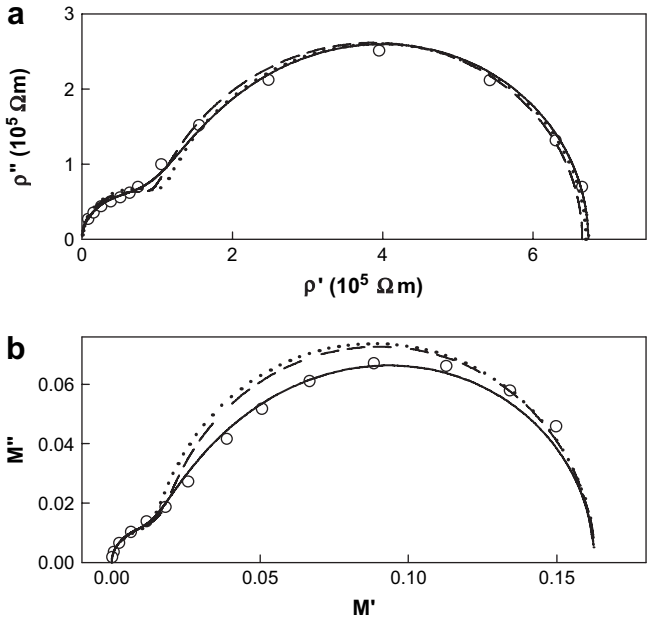

Fig. 4. Cole–Cole plots of (a) resistivity and (b) modulus for the 405 min spectra. Key: experimental (open circle), spherical amorphous inclusions (solid line), two layers (dashed line), crystalline shell–sphere (dotted line).

Table 1
The obtained model parameters[a]

Geometrical model	σ_m (S/m)	ϕ	ν
Spherical amorphous inclusions	1.73×10^{-5}	0.81	0.45
Shell–sphere	9.97×10^{-6}	0.72	0.67
Two layers in series	8.99×10^{-6}	0.70	0.85

[a] The permittivity values for the amorphous and crystalline phases are assumed to be the same and equal to 6.15.

crystalline and amorphous layers were arrayed randomly to the electric field, the spherical amorphous inclusion model performed better, showing that it adequately described the averaged dielectric behaviors.

Fig. 5 gives the details of the morphological evolution during recrystallization. The volume fraction of the semicrystalline particles, ϕ, was regarded as the dielectric analog of the volume fraction of spherulites in microscopic observations. ϕ increased with recrystallization time; it also looked like there were two rate constants; the volume fraction increased at a faster rate in the first stage, but it slowed down after ϕ exceeded 0.6. Yoo et al. suggested that there exist two morphologically different crystallites in PBSu [4]. The two rates could be associated with these two crystallites, which recrystallized at different times and at different rates. ϕ reached about 0.8 after the completion of recrystallization. ϕ did not extend to a full conversion because the recrystallization temperature was very close to the melting temperature. A higher ϕ value can only be

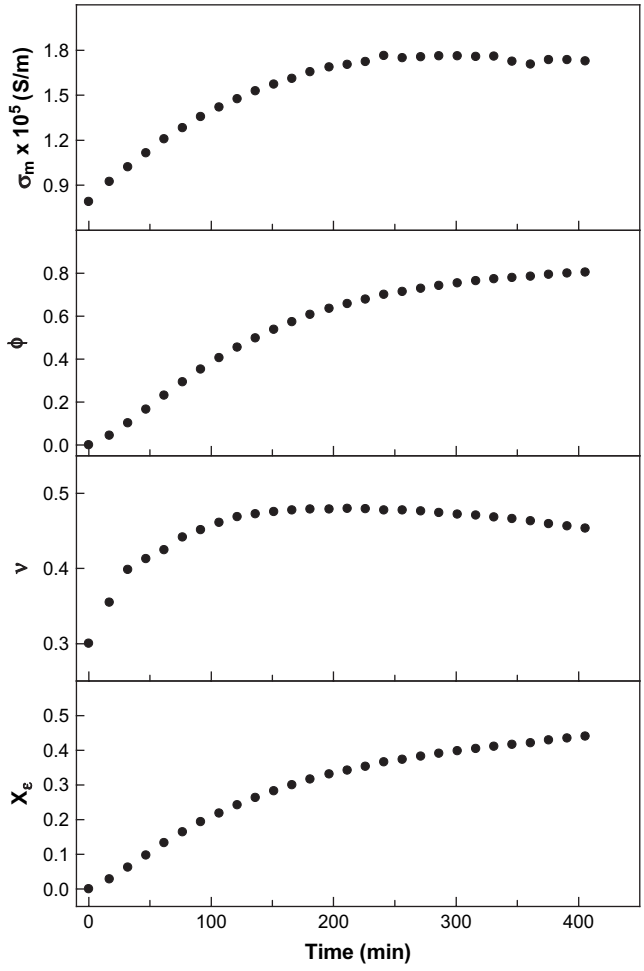

Fig. 5. Time dependence of the melt conductivity, σ_m, the volume fraction of the semicrystalline particles, ϕ, the amorphous fraction inside the particle, ν, and the bulk crystallinity, X_ε, during recrystallization at 383 K.

obtained by lowering the temperature. The change in the amorphous fraction of the particles, ν, was especially interesting. Strobl, in his observation of the buildup of spherulites under atomic force microscope, suggested that the sequential buildup of a spherulite begins with the fast growth of a few dominant lamellae and then continues with a much slower common growth of stacks of subsidiary lamellae [27]. In the case of the present study, the dielectric observation gave a similar and quantitative picture: the semicrystalline particle was highly crystalline when it was initially formed; the particle crystallinity dropped (ν increased) quickly in the first 100 min, from 0.7 to 0.5, then leveled off, followed by a very slow but steady trend of upturn. The faster growth of the dominant lamellae expanded the fraction of the particles, while the slower growth of the subsidiary lamellae could not keep up with the expansion of these particles; therefore the average particle crystallinity dropped in the beginning. With the considerable slowing down of the expansion of these semicrystalline particles came the increase of the particle crystallinity because of the growth of the subsidiary lamellae. The bulk crystallinity, X_ε, followed the trend in ϕ: two rate constants, a faster first-half increase rate followed by a slower second-half one. The behavior of the melt conductivity was also very interesting. One would imagine that because the bulk conductivity decreased with increased crystallinity, the conductivity in the unconverted portion would also decrease because of the restriction imposed by the crystals on the movement of charge species. However, the σ_m curve in Fig. 5 shows that as PBSu recrystallized, the ionic impurities were pushed away from the crystallization front, resulting in a melt with a higher concentration of ionic impurities and, consequently, a higher conductivity. σ_m leveled out in the middle of recrystallization, almost at the same time that ϕ entered its second stage of growth and the particle crystallinity began its slow but steady increase. The push of the slowly growing front (ϕ increased slowly) and the slow in-filling of the spherulite with growth of subsidiary lamellae (ν decreased slowly) that deterred the movement of charge species counterbalanced each other. Therefore, σ_m ceased to increase.

The intercept of the curve in the Cole–Cole plot of Fig. 3 with the real axis gives an estimate of bulk resistivity, and its reciprocal, bulk conductivity. The obtained value corresponds to σ_o in Eq. (2). One can ask if the bulk electrical properties of a semicrystalline polymer can be predicted from the properties of the constituent phases. There are many types of equations (mixing rules) that have been proposed for the prediction of the electrical conductivity of composite materials from those of their constituent phases [28]. Some of them are derived based on the Bruggeman–Hanai equation and successfully simulate the effective conductivity of a wide range of composite materials. In the case of semicrystalline polymers, however, few of these models have considered that the conductivity of the amorphous phase may change with crystallinity because of the expulsion of conducting species from the crystallizing phase. Therefore, it is difficult to establish an effective mixing rule for a property such as the electrical conductivity of a semicrystalline polymer, unless the relationship between the property of each constituent phase and the morphology is dealt with effectively.

4. Conclusions

PBSu exhibits a unique interfacial polarization phenomenon during recrystallization. This polarization arises from the high melt conductivity and the unique three-phase structure characteristic of the polymer melt dispersion of spherulites. Observing the polarization and the model fitting are best performed using the resistivity formalism. The relaxation behaviors can be successfully simulated using the Bruggeman–Hanai equation and a three-phase material model comprised of a melt matrix and spherical semicrystalline

particles with spherical amorphous inclusions. The melt conductivity increases with an increase in the overall degree of crystallinity, which shows that the concentration of the charge species in the melt increases as a result of rejection from the growing crystals. The particle crystallinity drops quickly first as the particle volume fraction increases at a high rate, and recovers slowly when the expansion of the semicrystalline particles slows down at the second stage.

Acknowledgements

The author gratefully acknowledges funding from National Science Council of the Republic of China (Grants NSC 92-2216-E-214-005).

References

[1] Yasuniwa M, Satou T. J Polym Sci Polym Phys Ed 2002;40(21):2411–20.
[2] Qiu Z, Komura M, Ikehara T, Nishi T. Polymer 2003;44(26):7781–5.
[3] Qiu Z, Ikehara T, Nishi T. Polymer 2003;44(10):3095–9.
[4] Yoo ES, Im SS. J Polym Sci Polym Phys Ed 1999;37(13):1357–66.
[5] Ichikawa Y, Suzuki J, Washiyama J, Moteki Y, Noguchi K, Okuyama K. Polymer 1994;35(15):3338–9.
[6] Ichikawa Y, Kondo H, Igarashi Y, Noguchi K, Okuyama K, Washiyama J. Polymer 2000;41(12):4719–27.
[7] Ihn KJ, Yoo ES, Im SS. Macromolecules 1995;28(7):2460–4.
[8] Tai H-J. Polymer 2007;48(15):4558–66.
[9] Asami K. J Phys D Appl Phys 2007;40(12):3718–27.
[10] Perrier G, Bergeret A. J Appl Phys 1995;77(6):2651–8.
[11] Furukawa T, Yasuda K, Takahashi Y. IEEE Trans DEI 2004;11(1):65–71.
[12] Lee Y-H, Bur AJ, Roth SC, Start PR, Harris RH. Polym Adv Technol 2005;16(2–3):249–56.
[13] Lei D, Runt J, Safari A, Newnham RE. Macromolecules 1987;20(8):1797–801.
[14] Hayward D, Pethrick RA, Siriwittayakorn T. Macromolecules 1992;25(5):1480–6.
[15] Hippel A. Dielectrics and waves. Boston: Artech House; 1995. p. 228–34.
[16] Fukao K, Miyamoto Y. J Non-Cryst Solids 1997;212(2–3):208–14.
[17] Fukao K, Miyamoto Y. Phys Rev Lett 1997;79(23):4613–6.
[18] Šics I, Nogales A, Ezquerra TA, Denchev Z, Baltá-Calleja FJ, Meyer A, et al. Rev Sci Instrum 2000;71(4):1733–6.
[19] Boyd RH, Liu F. In: Runt JP, Fitzgerald JJ, editors. Dielectric spectroscopy of polymeric materials. Washington DC: American Chemical Society; 1997 [chapter 4].
[20] Neagu E, Pissis P, Apekis L, Gomez Ribelles JL. J Phys D Appl Phys 1997;30(11):1551–60.
[21] Moynihan CT. Solid State Ionics 1998;105(1–4):175–83.
[22] Cirkel PA, van der Ploeg JPM, Koper GJM. Physica A; 235(1–2):269–278.
[23] Böttcher CJF, Bordewijk P. Theory of electric polarization, vol. II. Amsterdam: Elsevier Scientific Publishing Company; 1978. p. 476–87.
[24] Asami K. Prog Polym Sci 2002;27(8):1617–59.
[25] Boersma A, Wübbenhost M, van Turnhost J. Macromolecules 1997;30(10):2915–22.
[26] Hanai T. Kolloid Z 1960;171(1):23–31.
[27] Strobl G. Prog Polym Sci 2006;31(4):398–442.
[28] Niwas S, Gupta PK, de Lima OAL. Curr Sci India 2005;92(5):612–7.